CO_2 EOR by Diffusive Mixing in Fractured Reservoirs

Ø. Eide, G. Ersland, S. H .Lie, S. Baird, M. Haugen, T. Skagseth, A. Graue and M. A. Fernø
Department of Physics and Technology, University of Bergen, Norway

This paper was prepared for presentation at the International Symposium of the Society of Core Analysts held in Avignon, France, 7– 12 September, 2014.

Abstract

Miscible CO_2 flooding as an enhanced oil recovery (EOR) technique is currently employed in large parts of the US, and has a great potential. We here report on CO_2 injection in heterogeneous rock samples with fractures to study recoverable oil by diffusive mixing. In laboratory tests, CO_2 is injected through fractured core samples to displace oil. The injected CO_2 will follow the path of least resistance in the fracture, but the majority of oil is located in the oil-saturated matrix block adjacent to the CO_2-filled fracture. Oil is only produced by diffusion because the viscous forces are limited due to the high transmissibility of the fracture and the low viscosity of the injected CO_2.

Oil recovery by CO_2-oil diffusion in fractured core samples was visualized with nuclear magnetic resonance (MRI) and x-ray computed tomography (CT), both with and without residual water present. Oil recoveries above 90% OOIP were observed in several tests during injecting of several pore volumes CO_2. The presence of residual water reduced the rate of production by reducing the pore space and changed the tortuosity and CO_2 flow paths. The development of local CO_2 and oil saturations confirmed that diffusion was the main oil recovery mechanism, where oil was produced symmetrically from each side of the fracture along the length, without signs of viscous displacement. It was also revealed that diffusion produced oil from the inlet and outlet face of the core sample, which could not be captured from production measurements alone.

An effective diffusion coefficient was found using numerical simulation (CMG GEM) to reproduce the experimentally measured development in local CO2 and oil saturation. The validated numerical model was then used to perform a sensitivity analysis of important parameters such as sample size and porosity. Numerical simulations gave an effective molecular diffusion coefficient of $3.02 \cdot 10^{-9}$ m^2/s in homogeneous chalk samples and indicated a large degree of sensitivity to system size and tortuosity.

Introduction

In the US CO_2 injection for EOR has successfully been used for many years [6, 11-14]. This has been possible due to an abundance of CO_2 sources and relatively cheap field development and operation. Due to the large amount of pore volumes currently needed to do a successful CO_2 flood it has not been a viable option in an offshore environment. Next generation CO_2 flooding poses an opportunity for CO_2 injection in offshore environments, especially with increasing oil prices and increased government taxation of CO_2 release into the atmosphere. Economic incentives coupled with declining oil reserves, a lower rate of new discoveries and low recovery factors makes CO_2 a favorable injection fluid [7]. The North Sea is one of the areas with great potential for EOR and storage of CO_2. The challenge is capture and transportation from large

point sources located on shore. However, if CO_2 is made available for injection in reservoirs it may contribute significantly to a more effective and more sustainable energy production.

An important aspect to predict or optimize a CO_2 EOR projects is good experimental data that can be used to create reliable numerical models. In that regard, imaging the saturation development *in-situ* has been shown to be of great value. Imaging reveals the flow patterns of the different fluids [3], and makes it possible to separate effects that are important on the macro- and micro scale. There are several techniques to image saturation in the laboratory. The most important techniques are MRI and CT. CT uses the attenuation of x-rays in different materials to create 3D images. Attenuation is a function of molecular and atomic density. The main advantage of CT is that it images both the matrix and the fluids in the pore space. In order to map saturations with a CT scanner the fluids needs to have different attenuation and all of the phases need to be reference scanned at 100% saturation in the pore space.

MRI takes advantage of nuclear spin of protons in fluids to create images. Most MRIs are tuned to measure the spin of hydrogen nuclei. This enables the MRI to track oil and water and how they progress with time in a core sample. One advantage of MRI as it does not require reference scanning to quantify saturations, which simplifies experiments compared to CT experiments. Whereas CT imaging generally has better spatial resolution, MRI is more capable of characterization of fluids within sediments and signal response will vary with both density and viscosity. NMR T_2 mapping is commonly used to determine pore size distribution or fluid distribution on pore scale. Several MRI schemes (T_2, T_2-diffusion) have potential for characterization of complex miscible processes involving CO_2 and crude oils.

Experimental Procedure

Core Material

Experiments were conducted on a North Sea chalk field analogue. The Rørdal outcrop chalk, (quarried in Denmark) was selected because it is fairly homogeneous over a large number of samples, promoting repeatability between tests. It also has similar characteristics to several large fields in the North Sea, including Ekofisk and Eldfisk. The outcrop rock consists mainly of coccolith deposits and the composition is mainly calcite (99%) with some quartz (<1%). The porosity and permeability ranges between 43-47% and 2-5 mD, respectively. If the outcrop rock is not aged it is strongly water-wet with no spontaneous imbibition of oil [10]. More information can be found elsewhere [4, 9, 15, 16].

Core Preparation and Assembly

Core samples were cut from larger slabs of rock and dried at 80° C for several days before standard porosity and permeability measurements. One core sample was prepared without residual water, whereas irreducible water saturation was established in the other cores by bi-directional oil flooding at constant injection pressure. One core sample was aged with crude oil to near neutral-wet conditions. The core sample was first drained with crude oil to irreducible water saturation at constant injection pressure. The core sample was then flooded with crude oil at a continuous injection rate for several days. A more detailed explanation of the ageing procedure can be found in [8]. Before the experiments started all cores were cut in half in the longitudinal direction. This was done to create a large flow conduit for the injected CO_2 in the center of the cores. In one experiment the fracture was held open using a spacer, while in the others the

fracture was not held open. This resulted in permeability contrast between matrix and fracture of more than an order of magnitude with the spacer, and about 2 in the case of the closed fracture.

CO_2 Injection

One supercritical CO_2 injection test was performed at 40° C and 10 MPa and two liquid CO_2 injection tests were performed at 21° C and 10 MPa. To promote repeatability and to eliminate compositional effects between experiments, decane was used as the oil phase in all experiments. First contact miscibility between CO_2 and decane occurs at 8 MPa and 37.8° C [1]. At 21° C the MMP is approximately 5.4 MPa and at 40° C the MMP is approximately 9.2 MPa. This means that all experiments were conducted at first contact miscible conditions. The experimental setup is shown in Fig. 1. The experiments at liquid CO_2 conditions were imaged using MRI, while the experiment at supercritical CO_2 conditions were imaged using a medical CT-scanner. Apart from the core and fluid preheater used in the CT experiment, the experimental setup was identical in all experiments. All experiments were conducted with a net overburden stress of 1 MPa. To get quantitative images from the CT-scanner the core sample went through the following testing and imaging protocol:

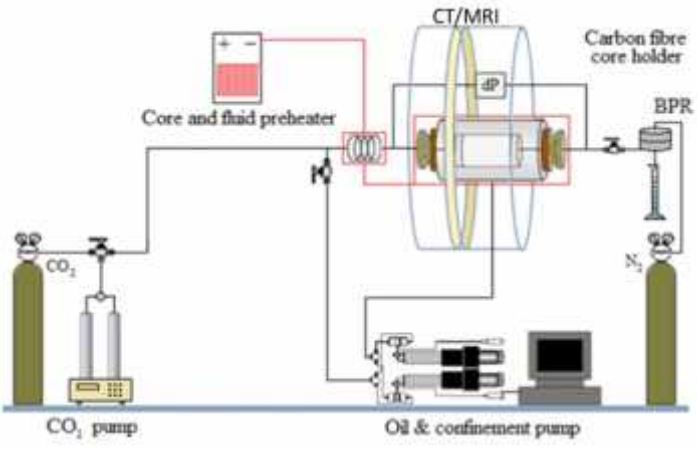

Figure 1: Schematic of the experimental setup, the core and fluid preheater was used in the CT-experiment. In the MRI-experiment the temperature was ambient.

- Flooded with CO_2 and imaged at experimental conditions
- Vacuum saturated with oil and imaged at experimental conditions
- Experiment was started and CO_2 was injected

In the 8.41 MHz MRI-scanner reference scanning was not necessary so the core sample was mounted in the scanner at residual water saturation. To avoid signal from both the water and the oil phase, deuterium oxide was used as the water phase. Deuterium oxide behaves very similarly to regular water in contact with CO_2, with slightly lower miscibility to CO_2 [2].

Results

Table 1 shows the results from standard core analysis as well as the final oil recovery factor after CO_2 injection. All core samples had a fracture running the length of the sample. In core sample RC#1 the fracture was held open using a 1 mm spacer, proving fracture permeability several orders of magnitude higher than the matrix permeability. In core samples RC#2 and 3 the fracture was not held open, meaning that the permeability contrast between the matrix and the fracture was about 2. This is sufficient to create a high conduit path for CO_2, meaning that there will be very limited viscous pressure. RC#1 was performed as a base line, and there was no water present in the experiment.

Table 1: Core properties

Core ID	Length [cm]	Radius [cm]	Porosity [%]	Matrix Permeability [mD]	Fracture Permeability [mD]	Irreducible Water Saturation [%]	Recovery Factor [% OOIP]
RC#1	8.0	2.5	46.8	3.6	-*	0	96.0
RC#2	6.0	1.9	46.9	3.1	6.2	27	95.5
RC#3	6.0	1.9	45.6	4.8	7.9	23	86.7

*Fracture permeability could not be accurately measured due to high conductivity in the fracture

X-ray Computed Tomography (CT) and Numerical Simulation

Fig. 2 shows the development in CO_2 saturation in core sample RC#1 seen with a bird's eye view. Warm colors indicate high oil saturation while cold colors represent low oil saturation. The color scale is shown at the bottom of the figure. Only the oil saturation is shown in the figure as the matrix has been cancelled out. Each image represents a single time step and because the average pore size is smaller than the voxel size, each voxel represents several pores. The fracture with the spacer runs through the middle of the core and the fracture volume is visible at 0.8 hours when CO_2 has displaced all the oil in the fracture. After 0.8 hours no more oil seems to be produced by viscous forces. This is because the oil saturation drops uniformly along the fracture during the rest of the experiment. The only exception is at 1/3 and 2/3 length of the sample. These are struts in the spacer to ensure the mechanical integrity of the system, and there is therefore a lower CO_2 concentration at those points in the fracture. Oil is also produced from the inlet and the outlet at the same rate. This is due to distribution caps at either end where CO_2 can accumulate. If there was a viscous component the oil should be produced from the inlet end first.

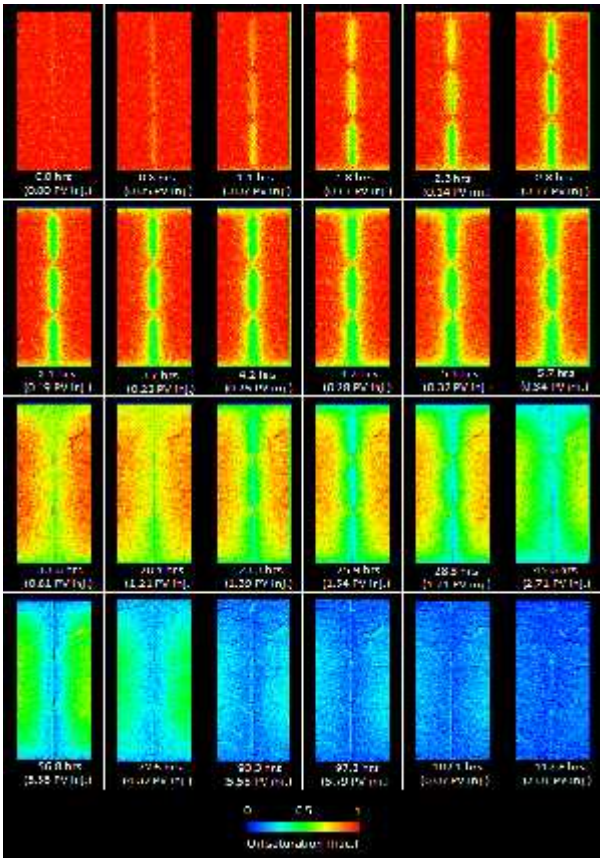

Figure 2: Oil saturation during CO2 injection in strongly water-wet core sample RC#1 with no water present. The core sample is shown in a bird's eye view with injection from the bottom of each picture.

Fig. 3 shows the development in the average oil saturation versus time. The experimental (black squares) and simulated (green) oil saturation profiles. A linear trendline (black, drawn) is fitted to the experimental data. The trendline had a slope of -0.094 and a R^2-value of 0.98, indicating a good fit to the experimental data. Note that there is a change in the slope between time 2 and 4. This is due to a slight drop in the ambient temperature which in turn lowered the density of CO_2 and caused a slight drop in CO_2 injection rate. This was only a problem at early times because the oil production rate dropped as the experiment continued. A numerical experiment was history matched to the experimental data using a diffusion coefficient of $3.02 \cdot 10^{-9}\ m^2/s$. The saturation data made it possible not only to match the material balance data, but also the *in-situ* saturation data. The simulation was carried

out using the CMG GEM compositional simulator. The model was made from a Cartesian grid with homogeneous matrix properties equal to the experimental conditions and a fracture with an infinite CO_2 volume and permeability several orders of magnitude higher than the matrix. An identical block was extracted from the *in-situ* data and provided the data which was matched against the model.

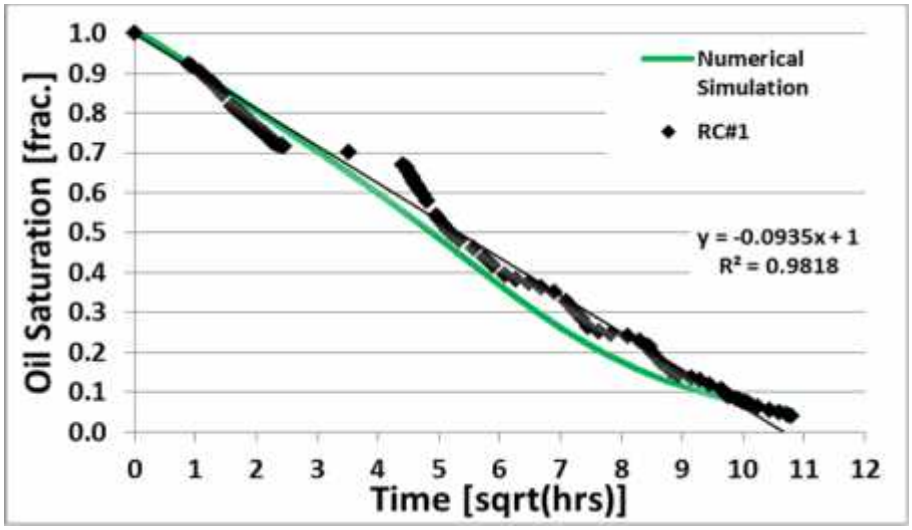

Figure 3: Oil saturation vs the square root of time during CO2 injection in strongly water-wet core sample RC#1 (black squares) as well as match from numerical simulation (green).

Sensitivity Analysis

Fig. 4 shows the numerical results demonstrating how changes in tortuosity impact the oil recovery rate during diffusive mixing.. All other parameters were kept constant. The final oil recovery is identical in all experiments; however the oil recovery rate is different. A higher tortuosity modifier results in higher tortuosity and thus longer diffusion length. As tortuosity goes down the diffusion length approaches bulk diffusion length.

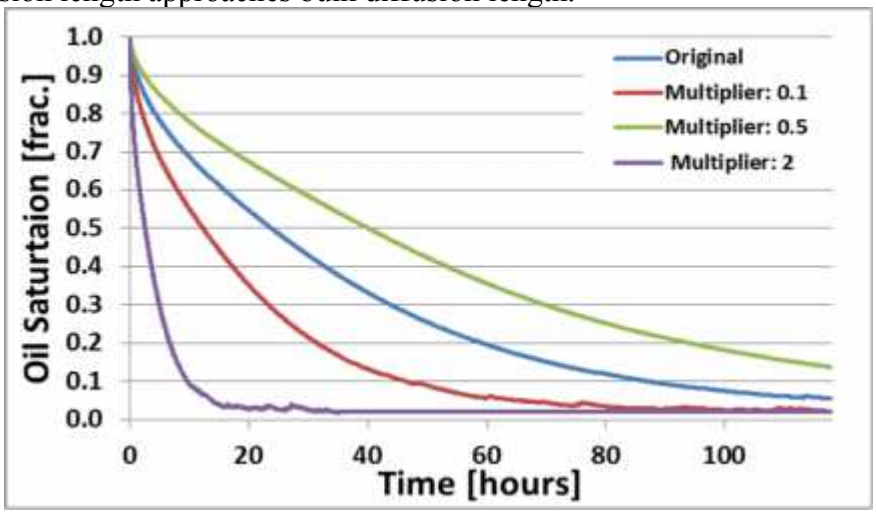

Figure 4: Oil saturation vs. time different tortuosity multipliers. The multipliers are indicated in the legend.

Sensitivity analysis for system size is shown in Fig. 5 as oil saturation versus time for different length scales. The ratio of length to width was identical in all the experiments, and the block size was increased. The model had an infinite amount of CO_2 in a fracture system surrounding the matrix. The final recovery was identical in all the simulations, but the oil recovery rate was different.

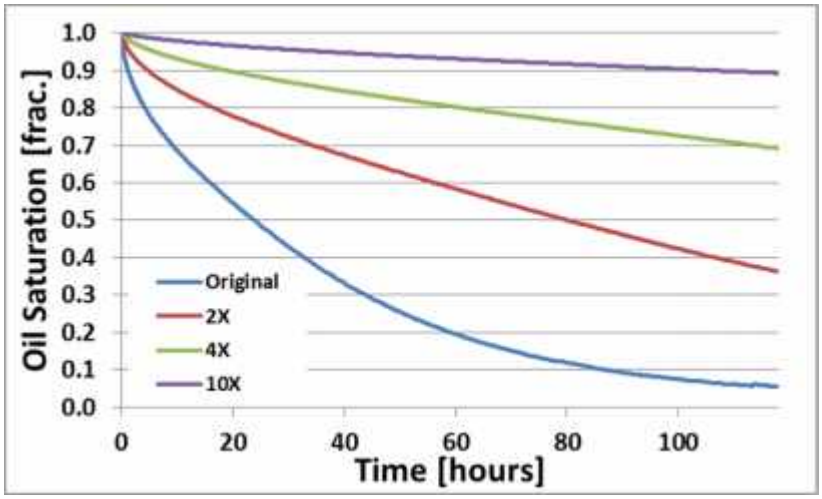

Figure 5: Oil saturation vs. time for different grid block size modifiers. Experimental conditions are shown in blue and the size modifiers are shown in the legend.

Nuclear Magnetic Resonance Imaging (MRI)

CO_2 injection in strongly water-wet core sample RC#2 is shown in Fig. 6. Fig. 6 shows a 3D representation of the core sample as it is mounted in the core holder. CO_2 is injected from the top and produced at the bottom and there is a closed fracture running the length of the sample parallel to the injection and production tubing shown in the figure. The entire signal is from the oil phase as the water phase (deuterium) and the rock do not give any signal in the MRI. As in the case of the CT-experiment, there does not seem to be a significant front moving through the system, and oil is produced from both the inlet end and the outlet end. The only exception is at early times where there is a slight front at the inlet. This is only visible until about 3.6 hours when oil starts being produced from the outlet as well.

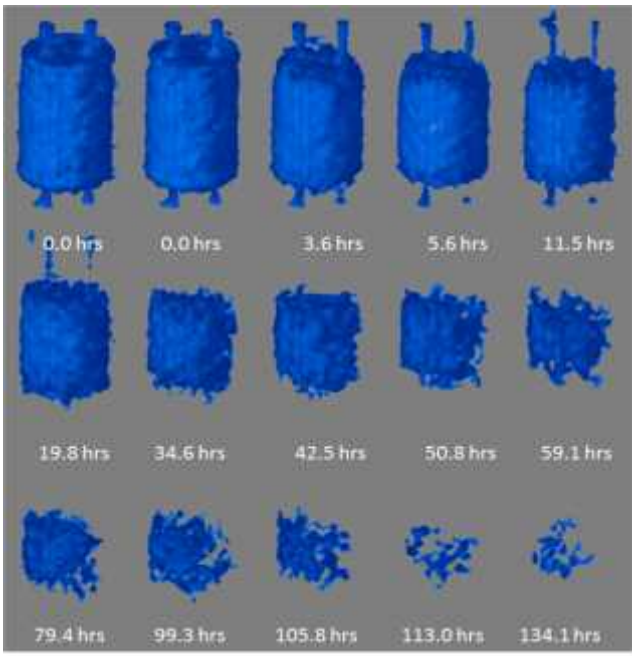

Figure 6: Oil saturation during CO2 injection in strongly water-wet core sample RC#2. Notice that the color map in Fig. 6 and Fig. 7 is different.

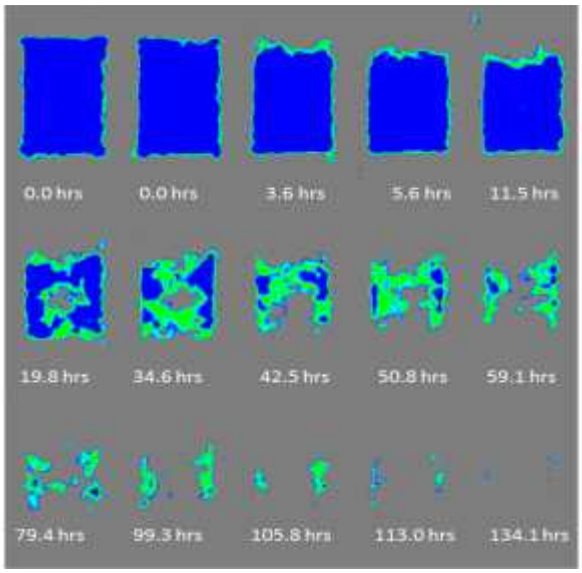

Figure 7: Oil saturation during CO_2 injection normal to the fracture plane in near neutral-wet core sample RC#2. Blue is high oil saturation and green is low oil saturation. Notice that the color map in Fig. 6 and Fig. 7 is different.

Fig. 7 shows core sample RC#2 in 2D during CO_2 injection. The view of the core sample is perpendicular to the fracture. Before 3.6 hours oil is mainly produced from the inlet end of the core sample. After 3.6 hours CO_2 has broken through the fracture and the oil saturation is dropping in the outlet end and around the fracture as well as the inlet. After 11.5 hours the largest drop in oil saturation occurs from the fracture into the matrix.

Fig. 8 shows the production profile for core sample RC#2 plotted as oil saturation versus the square root of time. A trendline is fitted to the data points in the area where the graph is linear. This was after time 5, the oil saturation at this time was 0.37. The linear trendline had a R^2-value of 0.97, which means that there is a good match between the experimental data and the linear fit, the slope of the trendline was -0.032. Before time 5 the graph is not linear so those points were not included in the trendline fit. A more thorough argument for this can be found in the discussion section. The experiment was stopped after 187 hours, at that point the oil saturation was 9% and the oil recovery was 87% of OOIP and 6.6 PVs of CO_2 had been injected. Note that no water was produced during CO_2 injection.

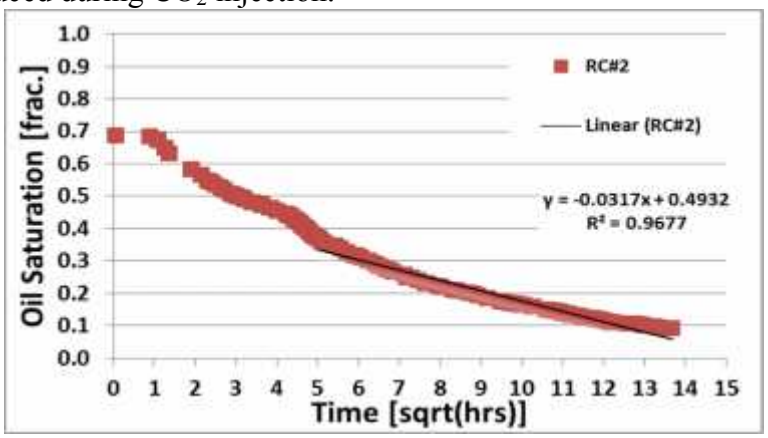

Figure 8: Oil saturation during CO2 injection in near neutral-wet core sample RC#3. A trendline is fitted to the linear part of the data.

Fig. 9 shows CO_2 injection in near neutral-wet core sample RC#3. Fig 9 shows a 3D representation of the core the way it was positioned in the core holder with CO_2 injected from the top. The fracture plane running the length of the sample was parallel to the injection tubing which is visible until 5.3 hours. The signal is from the oil phase only as the rock and the water phase (deuterium) are invisible to the MRI. In the experiment the CO_2 quickly displaced the oil in the fracture and oil was produced from the inlet, the outlet and along the fracture plane. This is visible from 22.2 hours when the two core halves separated by the fracture plane have become visible. At early times more oil was produced from the inlet end of the core sample. After 5.3 hours oil had broken through in the fracture and oil was produced both from the inlet and the outlet. After 33 hours most of the oil is produced along the fracture plane and not so much at the inlet and outlet.

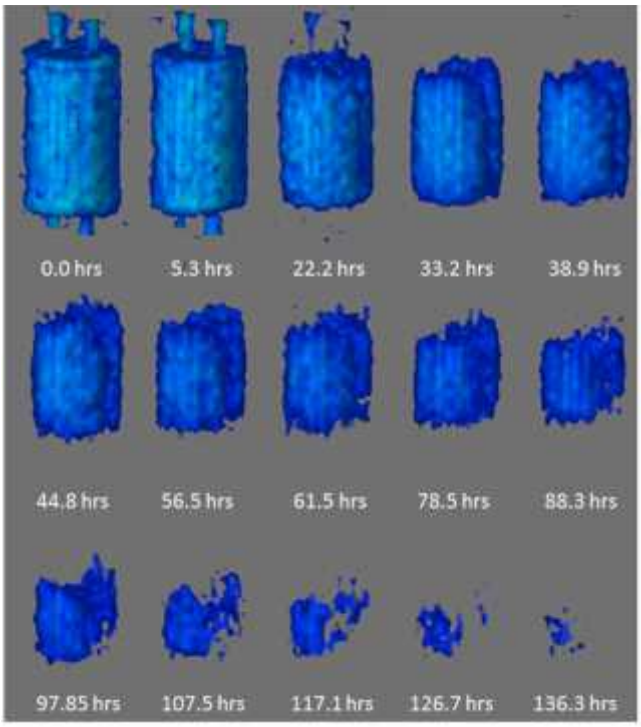

Figure 9: Oil saturation during CO2 injection in near neutral-wet core sample RC#3. Notice that the color map in Fig. 9 and Fig. 10 is different.

The CO_2 injection in near neutral-wet core RC#3 is shown in 2D in Fig. 10. The view of the core is perpendicular to the fracture, which is clearly visible after 117 hours. After 5.3 hours the CO_2 had broken through the fracture, and oil is being produced from the outlet of the core sample as

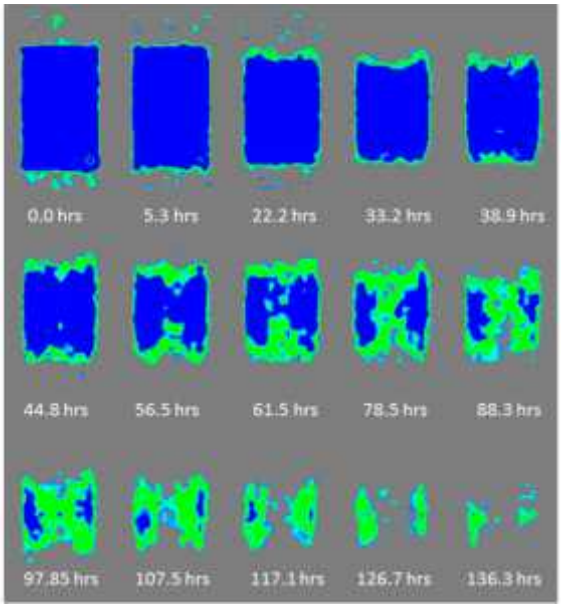

Figure 10: Oil saturation during CO2 injection normal to the fracture plane in near neutral-wet core sample RC#3. Blue is high oil saturation and green is low oil saturation. Notice that the color map in Fig. 9 and Fig. 10 is different.

well as the inlet. The production from the inlet and the outlet then slowed down and the fracture becomes visible after 38 hours. After that most of the oil seems to be produced from the matrix adjacent to the fracture, corroborating the data from the 3D images in Fig. 9.

Fig. 11 shows the oil production profile for near neutral-wet core RC#3, plotted as oil saturation versus the square root of time. A linear trendline is fitted to the experimental data after time 5 and oil saturation 0.31. The trendline had a R^2-value of 0.99 and a slope of -0.026. The trendline was only fitted to the linear part of the experimental data, a more thorough argument for this can be found in the discussion section. The experiment was ended after 144 hours, the oil saturation at termination of the experiment was 12% which correlates to an oil recovery of 85% OOIP. Oil was still being produced at termination, meaning that more oil could have been recovered if the experiment had continued. Note that no water was produced during CO_2 injection.

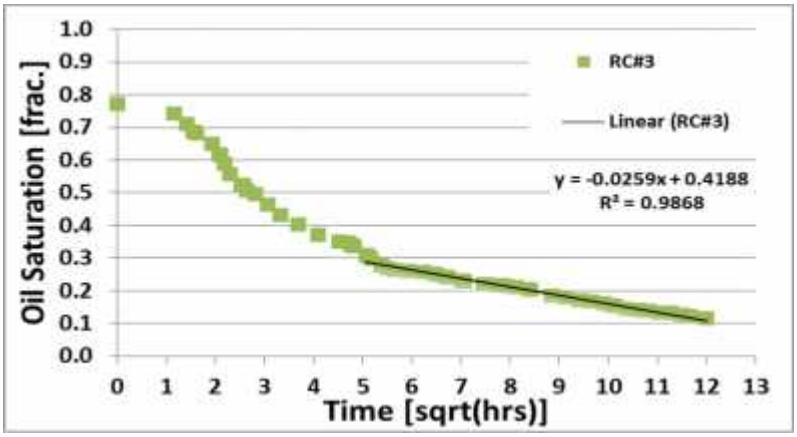

Figure 11: Oil saturation profile vs the square root of time during CO2 injection in near neutral-wet core sample RC#3. A trendline is fitted to the linear part of the data.

Fig. 12 shows the distribution of NMR T_2 relaxation times in core samples RC#2 (left) and RC#3 (right) at different time steps. The signal is only from the oil phase as the water phase is deuterium. In RC#2 the average relaxation in the oil peak was 488 ms. In RC#3 there seems to be a small peak just below 1 ms and the average relaxation at initial conditions was 280 ms. In the first 50 hours in RC#2 and 71 hours in RC#3 there is a shift towards longer relaxation times. This is likely due to decreased viscosity as CO_2 mixes and dilutes the oil phase. At 114 hours this trend is reversed in RC#2 and the relaxation times are decreasing with time. In RC#3 the last measurement at 148 hours also has lower relaxation compared with the previous scan.

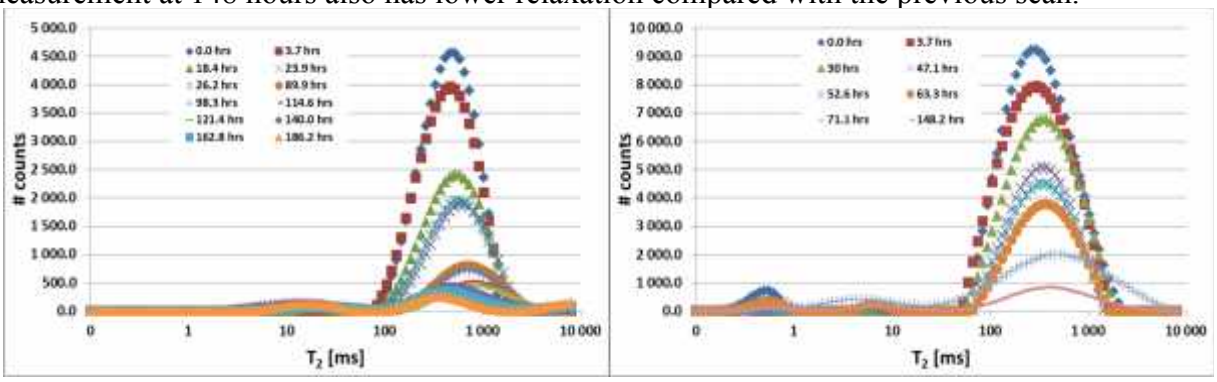

Figure 12: T2 spectrum from CMPG-sequence in core sample RC#2 (left) and RC#3 (right). The CMPG-sequence was taken at different time steps as indicated on the graphs.

Discussion

Production Mechanisms

A good fit between the production curve and the linear trendline shown in Fig. 5, 8 and 11 indicates that diffusion is the main production mechanism. Diffusion is described by Fick's law and if diffusion is the only production mechanism the saturation change should be linear with the square root of time. At the beginning of the CO_2 injection it is assumed that the oil in the fracture will be displaced by viscous forces. If the fracture permeability is low, some oil in the inlet end of the core would also be produced. This effect would be diminished once the CO_2 breaks through in the fracture due to the low viscosity of CO_2 compared to the oil. This effect is visible in Fig. 8 and Fig. 11 where the slope of the experimental data is more negative in the beginning before it becomes constant. This effect is also visible in Fig. 7 and 10 where oil is displaced from the inlet in the beginning before most of the oil is produced along the fracture plane. This effect is not visible in core sample RC#1 as seen in Fig. 2 and 3. The slope of the production profile (Fig. 3) is almost constant throughout the experiment, and the *in-situ* saturation data (Fig. 2) shows that no more oil is produced in the inlet end compared to the outlet end. We believe that is because the fracture in RC#2 and 3 has lower permeability than RC#1, meaning that diffusion will be the main production mechanism in RC#1 during the entire experiment. In RC#2 and 3 diffusion was the most important production mechanism after an initial period of viscous displacement. After this initial period of viscous displacement the slope of the experimental data becomes constant and a good fit between the linear trendline and the production data is made. This happens after time 5 in RC#2 and 3, which is after 24 hours.

Diffusion Rate

If the linear trendline from RC#1 is compared to the trendline of the diffusion dominated production from RC#2 and 3 it is apparent that the production rate (from diffusion) is different. With a slope of -0.094, RC#1 has the most negative slope and thus the highest diffusion rate. RC#2 and 3 has similar slopes during diffusion dominated production with slopes of -0.032 and -0.026, respectively. The difference between RC#1 and RC#2-3 is believed to be due to the absence of water in RC#1. Water in the pore system will decrease the contact surface between the oil and the CO_2. The diffusion of CO_2 in water is several orders of magnitude lower than CO_2 in oil, meaning that the water will effectively block the contact between CO_2 and oil. This effect is called water shielding. Not only will the surface area between the oil and the CO_2 be decreased, the effective tortuosity of the oil/CO_2 system will increase with the presence of water. This is corroborated by the numerical simulations in Fig. 4, the results show that increased tortuosity decreases the oil production rate. While the slope of RC#2 is 23% more negative than that of RC#3, this difference is not large enough to say something conclusive. The change in slope is believed to be due to the different water saturation and the distribution of water due to different wettability.

Effect of wettability

No clear effect of wettability can be seen in the material balance calculations, the 2D or 3D images. The CMPG-sequence, however, does reveal differences between RC#2 and 3, which is strongly water-wet and near neutral-wet, respectively. At initial conditions RC#2 has slower relaxation time in the oil peak compared to RC#3, this indicates that more of the oil is located in contact with the pore wall and less of the oil is in bulk phase [5]. This is consistent with the change in wettability to near neutral-wet conditions which causes the water and oil in the pore

space to rearrange. In core sample RC#3 a small peak can be detected at fast relaxation times. This is most likely due to not all of the water being replaced with deuterium oxide before the start of the experiment. It could also be caused by oil being in direct in contact with the pore wall as a result of the ageing. This oil would most likely be located in the pore throats and could explain the change in wetting characteristics to near neutral-wet. Wettability change in the pore throats would change the imbibition characteristics of the whole core sample and it would not spontaneously imbibe water. This is corroborated by the peak shifting to slower relaxation times as CO_2 is injected, consistent with the main peak.

At early times a lot of the oil is being produced by viscous displacement, which is the reason for the large drop in the number of counts in Fig. 10. At the same time the peak shifts to slower relaxation times, this is most likely due to decreased viscosity of the oil phase as it mixes with CO_2. At residual oil saturation (ca 150 hrs) the trend is reversed and there is a shift to faster relaxation times. This effect is more pronounced in RC#2 which is strongly water-wet. This may be explained by residual oil remaining close to the pore walls or that injected CO_2 was drying out water from the capillary bound wetting layer that coats the pore surfaces and shields the residual oil. In RC#3 much of the oil is already close to the pore wall due to the effects of ageing, making the effect of drying by CO_2 out less pronounced.

Effect of sample size

The effect of sample size can be seen clearly in Fig. 5, with high oil production rate at laboratory size, but as soon as the system size is increased the effect of diffusion becomes less significant. In addition, gravitational forces become more pronounced at larger system size, meaning that the production in Fig. 5 is not only due to diffusion. The effect of gravity increases with increased system size. This illustrates the importance of investigating the fundamental effects during laboratory experiments.

Conclusions

In situ imaging of CO_2 injections in fractured cores were carried out and the change in oil saturation was successfully spatially resolved using CT and MRI. In samples with high fracture permeability diffusion was the main oil recovery technique. With lower fracture permeability viscous displacement was the most important oil recovery at early times, and diffusion was the main oil recovery technique at late time. Numerical sensitivity shows that the effect of diffusion on the oil recovery will be more pronounced at laboratory-sized systems, and care must be taken when up-scaling results from laboratory experiments. Tortuosity was determined to be an important factor in the oil recovery rate by diffusion, as samples with high tortuosity in the oil phase had slower oil production rate. NMR spectroscopy revealed differences in the distribution of oil in the pore space at initial conditions. Shift in *T2* relaxation as CO_2 was injected indicated decreasing viscosity of the oil phase due to CO_2 dissolving in n-Decane.

Acknowledgements

The authors would like to thank the Norwegian Research Council for financial support. Statoil, BP and ConocoPhillips are also thanked for their financial contribution.

References

1. Ayirala, S.C., W. Xu and D.N. Rao, *Interfacial behaviour of complex hydrocarbon fluids at elevated pressures and temperatures.* Canadian Journal of Chemical Engineering, 2006. **84**(1): p. 22-32.
2. Curry, J. and C.L. Hazelton, *The Solubility of Carbon Dioxide in Deuterium Oxide at 25°1.* Journal of the American Chemical Society, 1938. **60**(11): p. 2771-2773.
3. Eide, Ø., M.A. Fernø, Z. Karpyn, Å. Haugen and A. Graue, *CO2 Injections for Enhanced Oil Recovery Visualized with an Industrial CT-scanner*, in *IOR 2013 - From Fundamental Science to Development*2013, EAGE: St. Petersburg, Russia.
4. Ekdale, A.A. and R.G. Bromley, *Trace Fossils and Ichnofabric in the Kjølby Gaard Marl, Uppermost Creataceous, Denmark.* Bull Geol. Soc. Denmark, 1993. **31**: p. 107-119.
5. Enick, R.M., D.K. Olsen, J.R. Ammer and W. Schuller, *mobility and conformance control for CO2 EOR via Thickeners, Foams and Gels - A literature review of 40 years of research and pilot tests*, in *SPE Improved Oil Recovery Symposium*2012, Society of Petroleum Engineers: Tulsa, Oklahoma, USA.
6. Enick, R.M.D.o.C.a.P.E., Univ. of Pittsburgh; D. Olsen, IBM Global Business Services; J. Ammer, US DOE National Energy Technology Laboratory; W. Schuller, URS Corporarion, *Mobility and Conformance Control for CO2 EOR via Thickeners, Foams, and Gels -- A Literature Review of 40 Years of Research and Pilot Tests*, in *SPE Improved Oil Recovery Symposium*2012, Society of Petroleum Engineers Tulsa, Oklahoma, USA.
7. Falcone, G. and R. Harrison, *Deciding Whether to Fund Either CCS or CCUS Offshore Projects: Are We Comparing Apples and Pears in the North Sea?*, in *SPE Annual Technical Conference and Exhibition*2013, 2013, Society of Petroleum Engineers: New Orleans, Louisiana, USA.
8. Graue, A., E. Aspenes, T. Bogno, R.W. Moe and J. Ramsdal, *Alteration of wettability and wettability heterogeneity.* Journal of Petroleum Science and Engineering, 2002. **33**(1-3): p. 3-17.
9. Hjuler, M.L., *Diagenesis of Upper Cretaceous onshore and offshore chalk from the North Sea area*, in *Institute of Environment & Resources*2007, Technical University of Denmark: Copenhagen, Denmark.
10. Johannesen, B., Else, *Wettability Determined by NMR and its Impacts on Oil Recovery in Chalk*, in *Institute for Physics and Technology*2008, University of Bergen: Bergen. p. 150.
11. Lambert, M.R., S.D. Marino, T.L. Anthony, M.W. Calvin, S. Gutierrez and D.P. Smith, *Implementing CO2 Floods: No More Delays!*, in *Permian Basin Oil and Gas Recovery Conference*1996, Society of Petroleum Engineers: Midland, Texas.
12. Leonard, J., *Annual Production Report.* Oil & Gas Journal, 1982.
13. Moritis, G., *Report on Enhanced Oil Recovery.* Oil & Gas Journal, 2004.
14. NETL, N.E.T.L., *Carbon Dioxide Enhanced Oil Recovery - Untapped Domestic Energy Supply and Long Term Carbon Storage Solution.* 2010(The Energy Lab).
15. Odling, N.E., P. Gillespie, B. Bourgine, C. Castaing, J.P. Chiles, N.P. Christensen, E. Fillion, A. Genter, C. Olsen, L. Thrane, R. Trice, E. Aarseth, J.J. Walsh and J. Watterson, *Variations in fracture system geometry and their implications for fluid flow in fractures hydrocarbon reservoirs.* Petroleum Geoscience, 1999. **5**(4): p. 373-384.
16. Strand, S., M.L. Hjuler, R. Torsvik, J.I. Pedersen, M.V. Madland and T. Austad, *Wettability of chalk: impact of silica, clay content and mechanical properties.* Petroleum Geoscience, 2007. **13**(1): p. 69-80.